Proceedings of ASME 2015 International Technical Conference and Exhibition & on Packaging and Integration of Electronic and Photonic Microsystems InterPACK2015 July 6-9, 2015, San Francisco, USA

InterPACKICNMM2015-48129

VALIDATION STUDY FOR VOF SIMULATIONS OF BOILING IN A MICROCHANNEL

Catherine Gorlé*, Hyoungsoon Lee, Farzad Houdhmand, Mehdi Asheghi, Kenneth Goodson
NanoHeat Lab
Department of Mechanical Engineering
Stanford University
Stanford, California 94305
Email: catherine.gorle@columbia.edu

Pritish R. Parida

IBM T.J. Watson Research Center
Yorktown Heights, New York, 10598
Email:prparida@us.ibm.com

ABSTRACT

This paper presents a comparison of Volume-of-Fluid simulation results with experiments [1] for two-phase flow and heat transfer in a micro channel. Mass transfer between the phases is modeled using a reduced-order model, requiring the definition of a time relaxation constant, r. A two-step solution procedure is used, where first a fixed temperature boundary condition is imposed at the heater to avoid overheating of the device during the initial development of the two-phase flow. After obtaining a quasi-steady-state solution this is changed to a heat flux boundary condition to determine the final solution. Results using three different values for r indicate that the value of the constant should vary throughout the domain. A final simulation where r is defined as a function of the streamwise location results in a prediction of the base temperature within 1K of the experimental result, a pressure drop within 30%, and a prediction of the location of transition from subcooled to saturated flow within 2mm.

NOMENCLATURE

c_p specific heat capacity at constant pressure [J/kg-K].
F_j Source term in the momentum equation [kg/m^2-s^2].
g_j Gravity [m/s^2].
h_{lv} Latent heat [J/kg].
K Thermal conductivity [W/m-K].
$\dot{m}_{lv}$ Mass transfer from liquid to vapor phase [kg/m^3-s].
$\dot{m}_{vl}$ Mass transfer from vapor to liquid phase [kg/m^3-s].
p Pressure [Pa].
p_{abs} Absolute pressure [Pa].
p_{sat} Saturation pressure [Pa].
r Time relaxation constant [1/s].
S_v Source term in the continuity equation [kg/m^3-s].
S_h Source term in the energy equation [W/m^3].
T Temperature [K].
T_{sat} Saturation temperature [K].
u_i i-th velocity component [m/s]
α_q Volume fraction of phase q [-].
κ Curvature [1/m].
σ_{vl} Surface tension coefficient [mN/m].
μ Dynamic viscosity [kg/m-s].
ρ Density [kg/m^3].
$_l$ liquid.
$_s$ solid.
$_v$ vapor.

INTRODUCTION

The development of next generation electronic and optoelectronic systems, telecommunication devices, and vehicle electron-

*Address all correspondence to this author. Present Address: Department of Civil Engineering and Engineering Mechanics, Columbia University, New York, NY, 10025

ics is driving an increasing interest in numerical models for two-phase flow in microfluidic geometries. While there has been significant progress in the development of computational methods and phase change models for comprehensive simulation of two-phase flows in compact geometries [2], the predictive capabilities of the computations should be carefully investigated for the different flow regimes of interest.

In this study we present a comparison of conjugate heat transfer Volume-of-fluid (VOF) simulation results with experimental data published in [1] for two-phase flow and heat transfer in a micro channel with a high exit vapor quality. The simulations are performed with Fluent v15.0.0, and the mass transfer between the phases is modeled using a reduced-order evaporation/condensation model [3] implemented in a user-defined-function. The model calculates the evaporation rate as a function of the difference between the local temperature and saturation temperature, and requires the definition of a time relaxation constant r that can strongly affect the results. More detailed models for the evaporation rate at liquid-vapor interfaces are available in literature [4–6], but the selected model is of interest for practical applications because of its simplicity, i.e. it does not require the calculation of the gradient of the volume fraction. The objective of this study is therefore to determine the capability of this modeling approach for predicting three engineering quantities of interest: the flow regime, the pressure drop and the temperature profile at the base of the micro channel.

The computational domain represents a single channel from the experimental set-up and includes half the width of the fins on either side of the channel, the silicon base, and the pyrex top layer to solve for conduction in the solid parts. A two-step solution procedure is used to efficiently solve the two-phase flow and conjugate heat transfer problem. The procedure avoids overheating the solid parts of the domain during the transient that occurs when the simulation is developing from the single-phase initial condition to a quasi-steady-state two-phase flow. The two steps use different boundary conditions for the lower wall: 1. a fixed temperature boundary condition to obtain an approximate initial solution for the two-phase flow and heat transfer, and 2. a heat flux boundary condition to reach the final quasi-steady-state solution. The influence of the time relaxation constant r is determined from simulations with three different values for r. In addition, one simulation with a value for r that increases with the downstream location in the channel was performed.

The following three sections of this paper provide a brief summary the experimental data set, a detailed description of the computational model, and a discussion of the simulation results that includes the comparison with the experimental data. The last section summarizes the conclusions and future work.

EXPERIMENTAL DATA SET

The experimental data set used in this validation study is available from [1], where it is labeled as a 'flashing two-phase flow without back flow' regime. The test case was selected for its relatively high exit vapor quality (24.2%). The largely saturated flow regime also implies that reasonably accurate predictions for the two-phase flow and heat transfer can most likely be obtained without detailed modeling of the nucleation sites and bubble growth in the first part of the channel.

The experimental set-up consists of 67 parallel channels separated by 50μm thick silicon walls. Each channel has a 100 by 100 μm cross-section and a length of 10mm, and an inlet orifice with a cross section of 50 by 100 μm and length 100μm. The device has a 380μm thick silicon base, which is heated at the bottom wall with a uniform heat flux of 47W/cm2, and the top consists of a 525 μm thick pyrex layer. The fluid is the refrigerant R245fa, and the mass flow rate per channel is 0.01895 g/s. The outlet manifold is kept at a temperature T of 304.65K, which corresponds to a saturation pressure p_{sat} of 187.48 kPa. The inlet manifold is sub-cooled by 7.2K, which corresponds to a temperature of 310.85K given the inlet manifold pressure of 293.48kPa.

The following three experimental results are available for comparison:

1. A flow visualization which indicates that the transition from bubbly to saturated flow occurs around 2.5 mm.
2. The pressure drop measured between the inlet and outlet plenum, which was equal to 106kPa, and the pressure drop between the channel inlet and outlet as determined from data reduction, which is reported as 68.2kPa.
3. An infrared temperature measurement of the base of the device. Figure 1 shows the span-wise average of the measured temperature profile along the channel.

COMPUTATIONAL MODEL

Governing Equations

The Volume of Fluid (VOF) method models two or more immiscible fluids by:

1. tracking the volume fraction of each of the fluids through the domain, where the volume fractions of all phases sum to unity.
2. solving a single set of momentum and energy equations where the fields for all variables and properties are shared by the phases and represent volume-averaged values.

For the volume fraction of fluid q, α_q, there are three possible states: $\alpha_q = 0$ when the cell is empty of fluid q, $\alpha_q = 1$ when the cell is full of fluid q, and $0 < \alpha_q < 1$ when the cell contains an interface between fluid q and another fluid. Based on the local

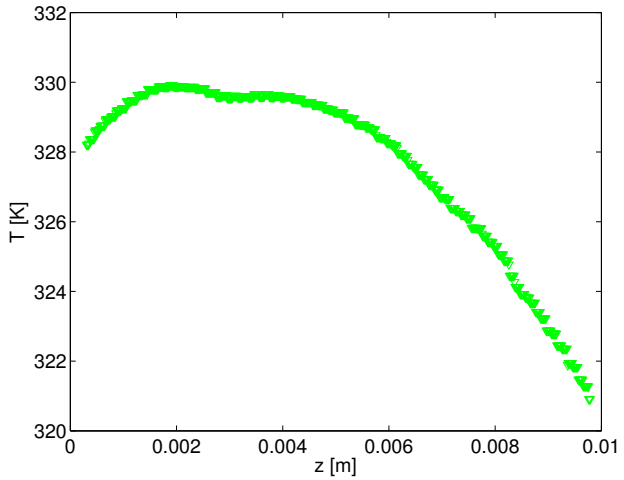

FIGURE 1. SPAN-WISE AVERAGED TEMPERATURE PROFILE ALONG THE TEST SECTION [1].

value of α_q the appropriate properties and variables will be assigned to each control volume. In the following we present the governing equations considering two phases, e.g. R245fa-liquid and R245fa-vapor.

Tracking of the interface between the phases is accomplished by the solution of a continuity equation for the volume fraction for the secondary phase. Defining the secondary phase as the vapor phase, α_v, this gives:

$$\frac{\partial}{\partial t}(\alpha_v \rho_v) + \frac{\partial}{\partial x_i}(\alpha_v \rho_v u_i)) = S_v + \dot{m}_{lv} - \dot{m}_{vl}, \quad (1)$$

where ρ_v is the vapor density, u_i is the i-th velocity component, S_v is a source term, $\dot{m}_{lv}$ is the mass transfer from the liquid to the vapor phase, and $\dot{m}_{vl}$ is the mass transfer from the vapor to the liquid phase. The primary (liquid) phase volume fraction α_l is computed using the constraint that the volume fractions of all phases sum to unity:

$$\alpha_v + \alpha_l = 1 \quad (2)$$

The mass transfer terms are modeled using the following reduced-order phase change model [3], which assumes that mass is transferred at a constant pressure and a quasi thermo-equilibrium state:

$$T \geq T_{sat} : \dot{m}_{lv} = r_l \rho_l \alpha_l (T - T_{sat})/T_{sat} \quad (3)$$
$$T \leq T_{sat} : \dot{m}_{vl} = r_v \rho_v \alpha_v (T - T_{sat})/T_{sat} \quad (4)$$

with T the temperature, T_{sat} the saturation temperature, r_v and r_l time relaxation constants, and ρ_l and ρ_v the liquid and vapor density. The model creates vapor mass fraction in any computational cell where the local temperature exceeds the saturation temperature, which is calculated based on the local absolute pressure p_{abs} [MPa] using the following relationship:

$$T_{sat} = 500.3299 p_{abs}^3 - 585.8015 p_{abs}^2 + 320.2113 p_{abs} - 11.2670 \quad (5)$$

A wide range of values for r_l and r_v, which determine the rate of evaporation and condensation, have been reported in literature. Most studies use $r = r_l = r_v$ and the values vary from 0.01s^{-1} in the original paper describing the model [3] to 100s^{-1} [7, 8] and even $7.5\text{e+}5\text{s}^{-1}$ [9]. In the present work it is also assumed that $r = r_l = r_v$ (condensation is not expected to play an important role), and three different values for r were used: 500, 1000, and 5000s^{-1}. When starting the simulations from a single phase initial condition the value for r is slowly increased to these final values to avoid numerical instabilities. While most previous studies have used values for r that are constant within the domain, the results of the present study will demonstrate that this assumption is not valid for the test case considered. Therefore, one final simulation with a value for r that increases with the downstream location in the channel was performed as well.

For the momentum and energy equations, the dependence on the volume fractions of the phases is included in the material properties that appear in the equations as volume-fraction-averages, and the resulting velocity and temperature fields are shared among both phases. A generic property γ is thus determined from the properties of the vapor (γ_v) and liquid (γ_l) phases as:

$$\gamma = \alpha_v \gamma_v + (1 - \alpha_v)\gamma_l \quad (6)$$

The momentum equation is given by:

$$\frac{\partial}{\partial t}(\rho u_j) + \frac{\partial}{\partial x_i}(\rho u_j u_i) = -\frac{\partial p}{\partial x_j} + \frac{\partial}{\partial x_i}\left[\mu\left(\frac{\partial u_j}{\partial x_i} + \frac{\partial u_i}{\partial x_j}\right)\right] + \rho g_j + F_j, \quad (7)$$

where ρ is the volume-averaged density, p the pressure and μ the volume-averaged dynamic viscosity. g_j represents gravity and F_j is a source term that includes the force induced by surface tension, which is modeled using the continuum surface force (CSF) model. The surface tension can be written in terms of the pressure jump across the surface. The force at the surface is then expressed as a volume force using the divergence theorem and

added in the momentum equations:

$$F_j = \sigma_{vl} \frac{\rho \kappa_v \frac{\partial \alpha_v}{\partial x_i}}{\frac{1}{2}(\rho_v + \rho_l)}, \tag{8}$$

where σ_{vl} is the surface tension coefficient, and κ_v is the curvature, which is defined in terms of the divergence of the unit normal. Wall adhesion effects are accounted for by specifying a wall adhesion angle. The contact angle that the fluid is assumed to make with the wall is used to adjust the surface normal in cells near the wall. This so-called dynamic boundary condition results in the adjustment of the curvature of the surface near the wall, which is used to adjust the body force term in the momentum equation.

The energy equation is given by:

$$\frac{\partial}{\partial t}(\rho c_p T) + \frac{\partial}{\partial x_i}(\rho c_p u_i T) = \frac{\partial}{\partial x_i}\left(K \frac{\partial T}{\partial x_i}\right) + S_h, \tag{9}$$

where c_p is the volume-averaged specific heat capacity at constant pressure, K the volume-averaged thermal conductivity, and S_h represents a source term, which includes the latent heat source related to the phase change:

$$S_h = -h(\dot{m}_{lv} - \dot{m}_{vl}), \tag{10}$$

with h the latent heat.

Finally, to account for the conjugate heat transfer, an additional energy equation is solved in the solid parts of the domain:

$$\frac{\partial}{\partial t}(\rho_s C_{p,s} T_s) = \frac{\partial}{\partial x_i}\left(K_s \frac{\partial T_s}{\partial x_i}\right), \tag{11}$$

where ρ_s is the solid density, $C_{p,s}$ is the specific heat capacity at constant pressure of the solid, K_s is the thermal conductivity of the solid material and T_s is the solid temperature.

Computational Domain and Boundary Conditions

The computational domain for the VOF simulation is shown in Fig. 2. The domain represents a single fluid channel, half the width of the silicon walls on either side of the channel, the silicon base, and the pyrex top layer. The fluid and solid properties are reported in Tab. 1. The fluid domain includes a small section of the inlet plenum, the inlet restriction, the main channel, and a small section of the outlet plenum. The dimensions are summarized in Tab. 2. By specifying adiabatic boundary conditions on the solid side (xz-plane) boundaries of the domain, and symmetry boundary conditions on the side (xz-plane) boundaries of the inlet and outlet plenum sections, the resulting simulation is representative of the flow in any of the channels in the experiment.

TABLE 1. FLUID AND SOLID PROPERTIES.

	Pyrex	Silicon
K_s W/m-K	1.1	149
ρ_s	2230	2330
$C_{p,s}$	753.12	703
R245fa	Vapor	Liquid
ρ [kg/m^3]	12.177	1309.8
C_p [J/kg-K]	993.29	1345.8
K [W/m-K]	0.0136	0.0842
μ [kg/m-s]	1.0783e-5	3.4885e-4
h_{lv} [J/kg]	184020.0	
σ [mN/m]	13.2	

TABLE 2. DIMENSIONS OF THE COMPUTATIONAL DOMAIN [μm].

	Length (x)	Width (y)	Depth (z)
Fluid inlet plenum	200	125	100
Fluid inlet restriction	100	50	100
Fluid channel	10000	100	100
Fluid outlet plenum	500	125	100
Silicon walls	10100	25*	100
Silicon base	10800	125	380
Pyrex top	10800	125	525
All	10800	125	1005

*50 at inlet restriction

At the inlet of the fluid channel, the mass flow is specified as 1.895e-5 kg/s, and the temperature of the liquid R245fa is set to 310.85K. At the outlet the pressure is fixed to -100kPa. For the fluid channel walls the 'coupled wall' boundary condition implemented in Fluent is specified, which uses a monolithic coupling

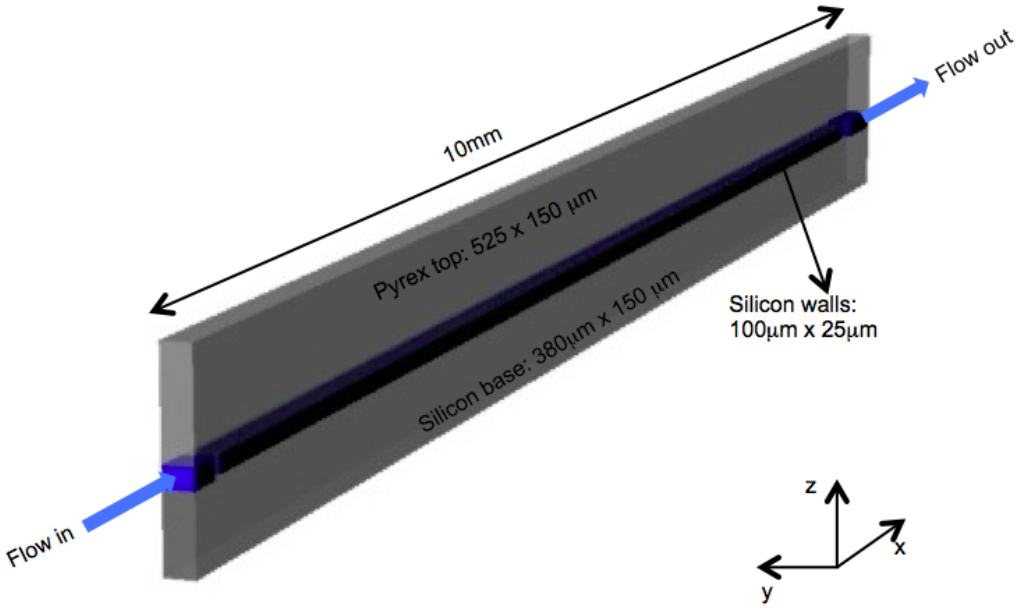

FIGURE 2. COMPUTATIONAL DOMAIN

approach that imposes continuity of temperatures and heat fluxes at the fluid-solid interfaces. The top (xy-plane) boundary of the pyrex layer is specified as a constant temperature boundary condition with T = 288.15K.

To enable efficiently solving the two-phase flow and conjugate heat transfer problem a two-step solution procedure is used. The procedure avoids overheating the solid parts of the domain during the initial transient that occurs in the simulation when the value of the time relaxation constant r is gradually increased to the desired value and the flow is developing from the single-phase initial condition to a quasi-steady-state two-phase flow. The two steps use different boundary conditions for the lower (xy-plane) wall:

1. A fixed temperature boundary condition, where the imposed temperature profile is extracted from the experimental data to obtain an approximate initial solution for the two-phase flow and heat transfer.
2. A heat flux boundary condition that imposes 47W/cm^2, corresponding to the value from the experiment, to determine the final quasi-steady-state solution for the flow and lower wall temperature.

The computational mesh consists of 3.7 million cells, with 1.3 million in the fluid domain. The near-wall resolution of the computational mesh in the fluid domain was defined to result in 5 cells within the first 8μm near the walls, which is the liquid film thickness estimated using published two-phase flow correlations [10, 11]. A grid dependency study is the focus of ongoing work.

Discretization Methods and Solution Procedure

The discretization of the volume fraction equation is done with the explicit scheme, which applies the standard finite-difference interpolation schemes to the volume fraction values computed at the previous time step. The face fluxes are obtained using the geometric reconstruction approach, i.e. the standard interpolation schemes are used for cells that are completely filled with one phase, while the geometric reconstruction (piecewise-linear) scheme is used for cells that are near the interface between the liquid and the vapor phase. The pressure-velocity coupling is done using the SIMPLE algorithm, the PRESTO! scheme is used for pressure, and second order upwind schemes are used for the discretization of the momentum and energy equations. Gradients are computed using a least squares cell based approximation. A first order implicit variable time stepping method is used, and the value of the maximum time step is limited by specifying a maximum global Courant number of 2. The resulting time step varied from around 1.0e-05s initially to 1.0e-07s throughout the simulation.The required decrease in the time step was related to an increase in the vapor fraction in the domain, which is directly related to the value specified for the time relaxation constant in the phase change model. A maximum of 20 iterations per time step was allowed, but on average only 5 iterations per time step were required to reach the convergence criterium for the residu-

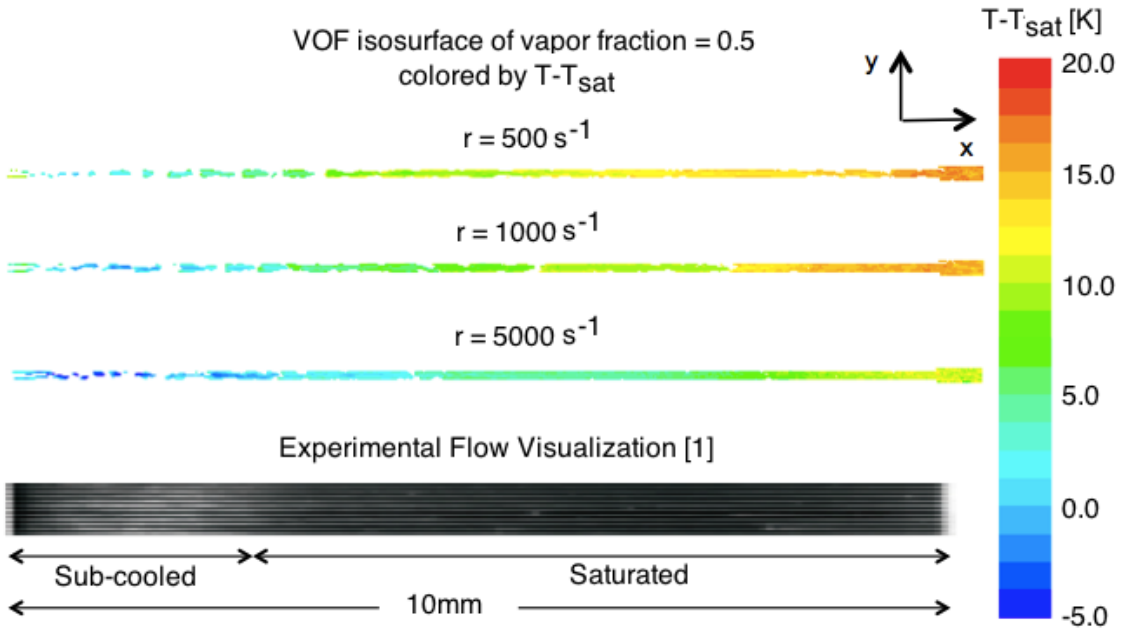

FIGURE 3. COMPARISON OF NUMERICAL AND EXPERIMENTAL [1] FLOW REGIME FOR VOF SIMULATIONS WITH CONSTANT TEMPERATURE BOUNDARY CONDITIONS USING DIFFERENT VALUES FOR r

als, which was specified as 10^{-3} for continuity and momentum and 10^{-6} for energy. The simulations were run in parallel on 48 processors, and required approximately 24 hours to compute 6000 time steps, which corresponds to a flow time of $1.2e-3s$.

RESULTS

The following subsection presents the results for the first step in the solution procedure, where the fixed temperature boundary condition was used for three different values of r (500, 1000 and 5000s^{-1}). Subsequently the evolution of the temperature at the base of the device when switching to the heat flux boundary condition in the second step is discussed for each of the r values. Based on these results a function for r was derived, which specifies an increase in the value when moving downstream in the domain. The results of this final simulation are presented in the last subsection.

Results using Fixed Temperature Boundary Condition for Three Different Time Relaxation Constants

During the first step of the solution procedure the temperature at the base of the device was specified to be equal to a polynomial fit to the experimental profile shown in Fig. 1, and the results presented focus on the flow pattern and the pressure drop. The simulations were run until a quasi-steady state solution was obtained, which was verified by monitoring the pressure drop between the channel inlet and outlet.

Figure 3 presents a comparison of the flow visualization from the VOF simulations using the three different r values and the experiments. For the VOF simulations the flow is visualized using an instantaneous plot of the iso-surface of the vapor volume fraction equal to 0.5. The transition between bubbly and annular flow regimes in the simulations is observed between 2.5 and 4.0mm, with the earliest transition occurring for the highest evaporation rate, i.e. for r = 5000s^{-1}. This corresponds best to the experimental transition location, which is identified around 2.5mm where the flow visualization transitions from light to dark gray. The iso-surface is colored by the difference between the local temperature and the saturation temperature to indicate whether the evaporation rate is maintaining the interface temperature close to the saturation temperature. It is shown that increasing r decreases deviations of the interface temperature from the saturation temperature, i.e. for r = 5000s^{-1} the lowest difference between the interface and the saturation temperature is obtained in the downstream part of the computational domain.. The fact that the discrepancy is negative upstream and positive downstream is a first indication that r should be variable in the downstream direction.

The pressure drops, reported in Tab. 3, show that for the highest value of r the pressure drop is over predicted by more than 100%, while for r = 500s^{-1} the pressure drop is within the uncertainty interval reported in the experiment.

TABLE 3. COMPARISON OF TIME AVERAGED NUMERICAL AND EXPERIMENTAL [1] PRESSURE DROP [kPa] FOR VOF SIMULATIONS WITH CONSTANT TEMPERATURE BOUNDARY CONDITIONS USING DIFFERENT VALUES FOR r

Experiment		68.2 ± 4.2
VOF	$r = 500$	70.2
	$r = 1000$	87.5
	$r = 5000$	133.2

Results using Heat Flux Boundary Condition for Three Different Time Relaxation Constants

In the second step of the solution procedure the constant temperature boundary condition was changed to a heat flux boundary condition imposing 47W/cm^2, corresponding to the experiment. The flow regime was found to be very similar to Fig. 3, and the pressure drop remained within 5kPa of the values reported in Tab. 3. The temperature at the base of the device did start to deviate from the previously imposed polynomial fit and the evolution of the temperature during the first 12000 time steps of the simulations is shown in Fig. 4 at intervals of 2000 time steps. The plots show that for all values of r the temperature decreases in the most upstream part of the domain, indicating that too much evaporative cooling occurs. The decrease is stronger for the highest value of r, i.e. for the highest evaporation rate. In the downstream part of the domain the opposite trend is observed: the temperature increases for all r values, but the increase is largest for the lowest value of r. Within the 12000 time steps reported here, none of the simulations reached a quasi-steady-state condition, but there is one location in the domain where the temperature remains constant for all three simulations, and that location moves further downstream as r increases. These observations confirm that a constant value of the time relaxation constant r is not appropriate for representing the different flow regimes in the channel.

Results using Heat Flux Boundary Condition and Variable Time Relaxation Constant

Based on the results obtained using the different constant values for the time relaxation constant, one simulation where r is a function of the streamwise location in the channel, as shown in Fig. 5, was performed. The function was defined to be equal to 500, 1000 and 5000 at approximately 4.5, 5.0 and 7.5mm downstream of the inlet respectively, which corresponds to the locations where a limited change in the temperature was observed in Fig. 4. The inlet and outlet values were set to 1 and 10000. We note that this function was derived for the specific test case under consideration, and that it has not been tuned to provide good

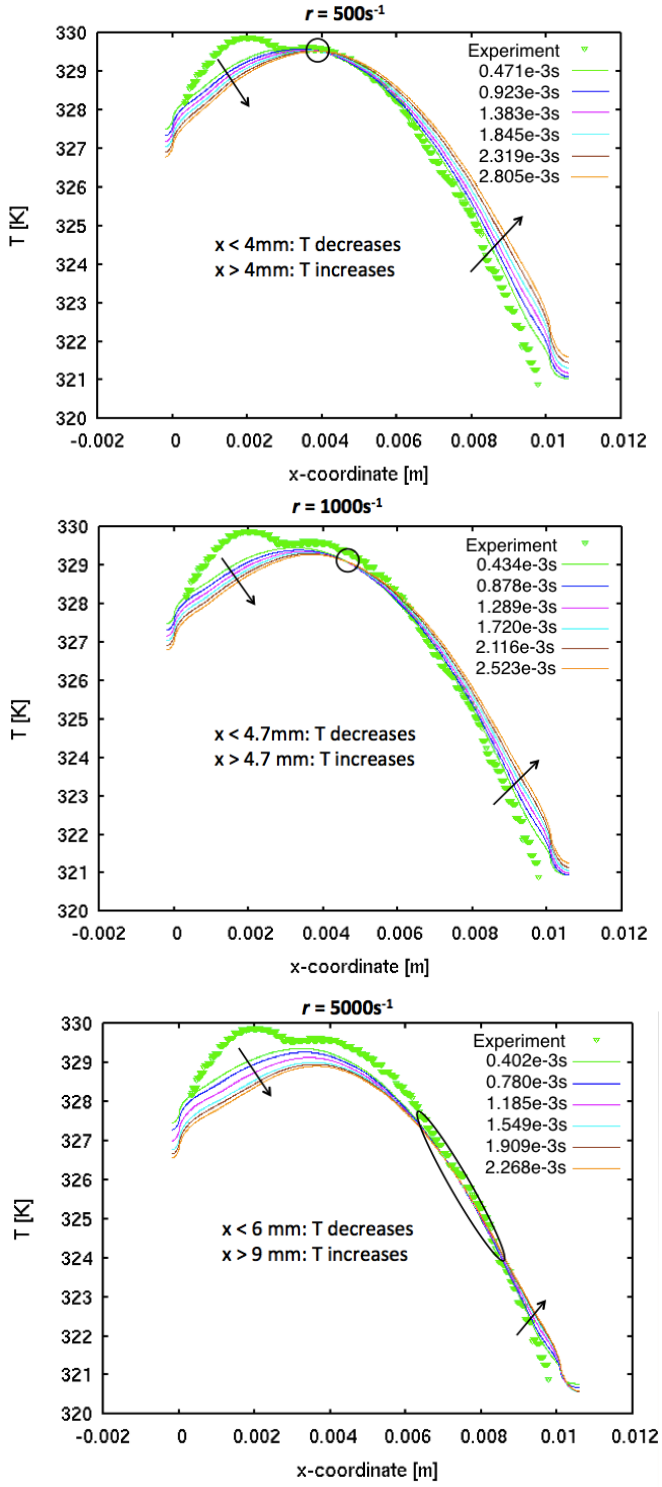

FIGURE 4. TEMPERATURE EVOLUTION AT THE BASE FOR VOF SIMULATIONS WITH DIFFERENT VALUES FOR r AND COMPARISON WITH EXPERIMENT [1]

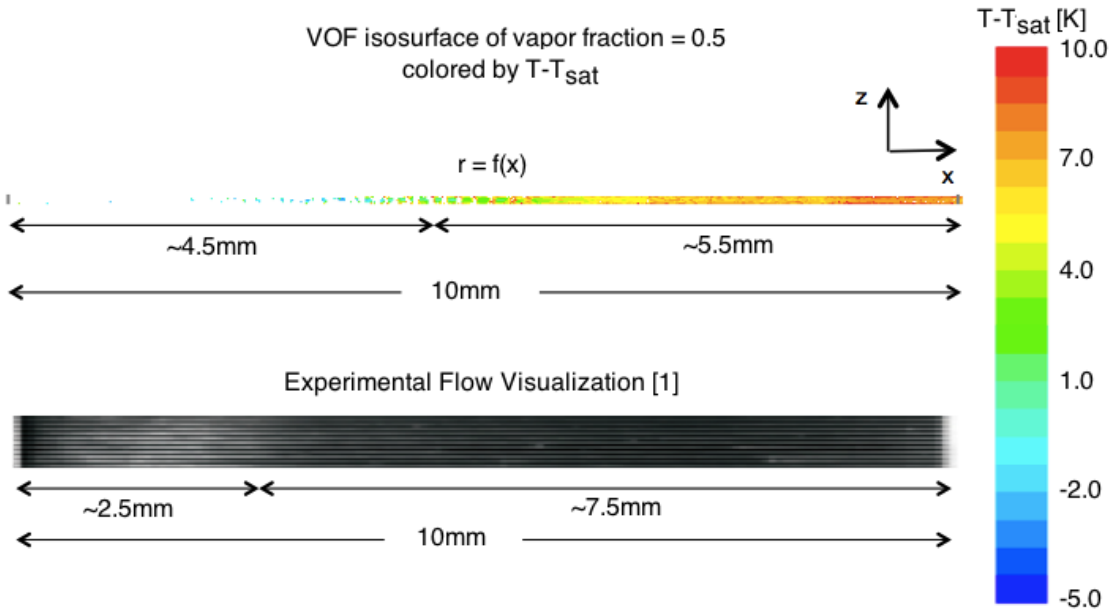

FIGURE 6. COMPARISON OF NUMERICAL AND EXPERIMENTAL [1] FLOW REGIME FOR VOF SIMULATIONS WITH HEAT FLUX BOUNDARY CONDITIONS AND VARIABLE r

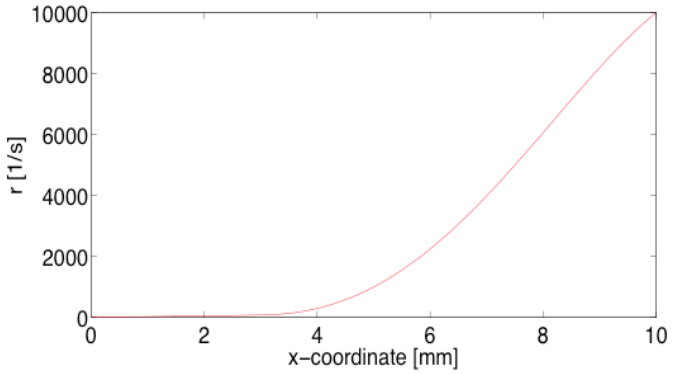

FIGURE 5. TIME RELAXATION CONSTANT AS A FUNCTION OF THE STREAMWISE LOCATION

agreement with the test data. Therefore, it does not represent a universal or optimal relationship for r, but it does serve our purpose of investigating the possible improvement that can be obtained by specifying r as a function of the downstream distance.

Figure 6 presents the comparison of the flow visualization, which shows that the difference between the interface temperature and the saturation temperature has been reduced compared to Fig. 3. The prediction of the transition from a bubbly to an annular flow occurs at around 4.5mm, which is within 2mm of the experimental observation.

Figure 7 presents the comparison of the temperature evolution when changing from the constant temperature to the heat flux boundary condition. The plot shows that the temperature

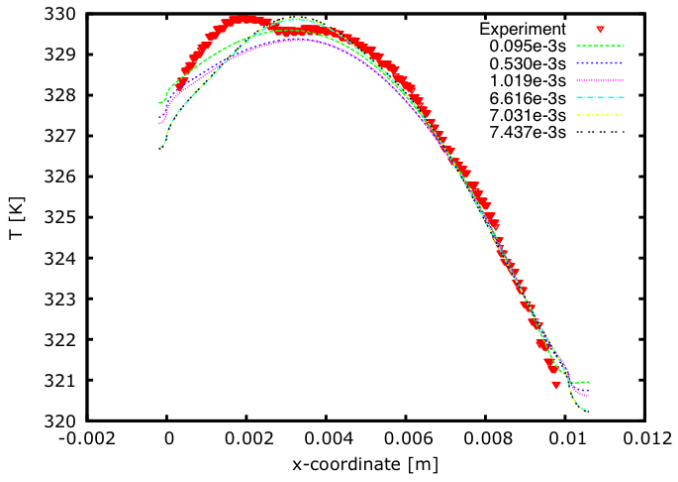

FIGURE 7. TEMPERATURE EVOLUTION AT THE BASE FOR VOF SIMULATIONS WITH VARIABLE r AND COMPARISON WITH EXPERIMENT [1]

TABLE 4. COMPARISON OF TIME AVERAGED NUMERICAL AND EXPERIMENTAL [1] PRESSURE DROP [kPa] FOR VOF SIMULATIONS WITH VARIABLE r

Experiment		68.2 ± 4.2
VOF	$r = f(x)$	88.8

still decreases in the most upstream part of the channel, but after a sufficiently long simulation time it converges towards a quasi-steady-state solution which is within 1K of the experimental temperature profile along the entire length of the channel. Finally, Tab. 4 reports the comparison of the pressure drop, indicating that the predicted pressure drop is within 30% of the experimental result.

CONCLUSIONS AND FUTURE WORK

Conjugate heat transfer VOF simulations for two-phase cooling in a micro-channel have been performed with the commercial solver Fluent v15.0.0 and the results have been compared to experimental data from [1]. Mass transfer between the phases was modeled using a reduced-order model, requiring the definition of a time relaxation constant, r, and the influence of this constant on the solution was investigated by performing simulations for r = 500, 1000 and 5000s^{-1}.

To enable efficiently solving the two-phase flow and conjugate heat transfer problem a two-step solution procedure was used. The procedure avoids overheating the solid parts of the domain during the initial transient that occurs when the flow is developing from the single-phase initial condition to a quasi-steady-state two-phase flow. The two steps impose different boundary conditions at the lower wall, where first a quasi-steady-state two-phase flow solution is obtained using a fixed temperature boundary condition, which was extracted from the experimental data, and second a heat flux boundary condition corresponding to the value from the experiment is imposed to calculate the final quasi-steady-state flow solution and lower wall temperature.

Results for both steps using three different values for r indicated that the value of the constant should vary throughout the domain. A final simulation where r was defined as a function of the streamwise location was shown to result in a prediction of the base temperature within 1K of the experimental result, a pressure drop within 30%, and a prediction of the location of transition from subcooled to saturated flow within 2mm.

Ongoing work is focussing on a several model improvements. First, a boundary condition which updates the outlet pressure as a function of the calculated pressure drop will be implemented to ensure maintaining the correct sub-cooling at the inlet. Second, the initial estimate of the temperature boundary condition imposed in step 1. will be based on results obtained from a reduced-physics model [12]. Finally, instead of specifying an approximate function for the time-relaxation constant based on observations from simulations for different constant values of r, physics-based relationships will be considered. On the long term, investigating a decoupling of the fluid and solid time stepping would be a valuable contribution for conjugate heat transfer simulations, since this could considerably reduce the computational time, in particular for cases where an accurate initial estimate of the solid temperature is unavailable.

ACKNOWLEDGMENT

This project was supported in part by the U.S. Defense Advanced Research Projects Agency Microsystems Technology Office ICECool Fundamentals Program under award number HR0011-13-C-0035. Disclaimer: The views, opinions, and/or findings contained in this article/presentation are those of the author/presenter and should not be interpreted as representing the official views or policies, either expressed or implied of the Defense Advanced Research Projects Agency or Department of Defense.

REFERENCES

[1] Szczukiewicz, S., 2012. "Thermal and Visual Operational Characteristics of Multi-Microchannel Evaporators using Refrigerants". PhD Thesis, Ecole Polytechnique Federale de Lausanne, Lausanne, EPFL, November.

[2] Szczukiewicz, S., Magnini, M., and Thome, J., 2014. "Proposed models, ongoing experiments, and latest numerical simulations of microchannel two-phase flow boiling". *International Journal of Multiphase Flow,* ***59***, pp. 84–101.

[3] Lee, W., 1980. "A pressure iteration scheme for two-phase flow modeling". In *Multiphase transport fundamentals, reactor safety, applications*, T. Veziroglu, ed. Hemisphere Publishing, Washington DC.

[4] Schrage, R., 1953. *A theoretical study of interphase mass transfer*. Columbia University Press, New York.

[5] Tanasawa, I., 1991. "Advances in condensation heat transfer". In Advances in Heat Transfer, J. Hartnett and T. Irvine, eds., Academic Press.

[6] Hardt, S., and Wondra, F., 2008. "Evaporation model for interfacial flows based on a continuum-field representation of the source terms". *Journal of Computational Physics,* ***227***, pp. 5871–5895.

[7] Yang, Z., Peng, X., and Ye, P., 2008. "Numerical and experimental investigation of two phase flow during boiling in a coiled tube". *International Journal of Heat and Mass Transfer,* ***51***, pp. 1003–1016.

[8] Fang, C., David, M., Rogacs, A., and Goodson, K., 2010. "Volume of fluid simulation of boiling two phase flow in a

vapor-venting microchannel". *Frontiers of Heat and Mass Transfer,* ***1***, pp. 1–11.

[9] Riva, E. D., and Col, D. D., 2011. "Effect of gravity during condensation of r134a in a circular minichannel". *Journal of Microgravity Science and Technology,* ***23***, pp. 87–97.

[10] Cioncolini, A., and Thome, J., 2011. "Algebraic turbulence modeling in adiabatic and evaporating annular two-phase flow". *International Journal of Heat and Fluid Flow,* ***32***, pp. 805–817.

[11] Cioncolini, A., and d'Entremont, B., 2014. Unified annular flow models. On the WWW, August. URL `http://2phaseflow.org/active:annularmodels`.

[12] Parida, P. "Reduced order modeling for chip-embedded micro-channel flow boiling". *Proceedings of the ASME 2015 International Technical Conference and Exhibition on Packaging and Integration of Electronic and Photonic Microsystems and ASME 2015 13th International Conference on Nanochannels, Microchannels, and Minichannels InterPACKICNMM2015*.